Published in final edited form as:

J Biol Inorg Chem. 2015 July ; 20(5): 875–883. doi:10.1007/s00775-015-1272-4.

Oxidized and Reduced [2Fe-2S] Clusters from an Iron(I) Synthon

Megan E. Reesbeck[†], **Meghan M. Rodriguez**[‡], **William W. Brennessel**[‡], **Brandon Q. Mercado**[†], **David Vinyard**[†], and **Patrick L. Holland**[†,]

[†]Department of Chemistry, Yale University, 225 Prospect Street, New Haven, Connecticut 06520, United States

[‡]Department of Chemistry, University of Rochester, 120 Trustee Road, Rochester, New York 14627, United States

Abstract

Synthetic [2Fe-2S] clusters are often used to elucidate ligand effects on the reduction potentials and spectroscopy of natural electron transfer sites, which can have anionic Cys ligands or neutral His ligands. Current synthetic routes to [2Fe-2S] clusters are limited in their feasibility with a range of supporting ligands. Here we report a new synthetic route to synthetic [2Fe-2S] clusters, through oxidation of an iron(I) source with elemental sulfur. This method yields a neutral diketiminate-supported [2Fe-2S] cluster in the diiron(III) oxidized form. The oxidized [2Fe-2S] cluster can be reduced to a mixed valent iron(II)-iron(III) compound. Both the diferric and reduced mixed valent clusters are characterized using X-ray crystallography, Mössbauer spectroscopy, EPR spectroscopy and cyclic voltammetry. The reduced compound is particularly interesting because its X-ray crystal structure shows a difference in Fe-S bond lengths to one of the iron atoms, consistent with valence localization. The valence localization is also evident from Mössbauer spectroscopy.

Keywords

Iron sulfur cluster; Mössbauer spectroscopy; diketiminate; model cluster; mixed valence

Introduction

Iron-sulfur clusters primarily function in electron transfer roles [1,2,3,4,5]. Their ability to accept and discharge electrons quickly is related to the small reorganization energy between redox states [6,7]. The [2Fe-2S] clusters typically cycle between an oxidized diferric state ($2Fe^{3+}$) and a one electron reduced state ($Fe^{2+}Fe^{3+}$). Ferredoxin type [2Fe-2S] clusters are ligated by four cysteine residues, and Rieske type clusters have one iron ligated by two histidines (Figure 1) [8,9]. MitoNEET has a new type of [2Fe-2S] cluster, which is coordinated by three cysteines and one histidine (Figure 1) [10]. The influences of first- and second-sphere amino acid residues on the redox potentials of these clusters have been studied using mutations [11,12,13,14,15].

Patrick.holland@yale.edu.

In order to provide fundamental information on the properties of these clusters in the absence of the protein scaffold, synthetic chemists have prepared many [2Fe-2S] clusters [8]. Synthetic clusters help to elucidate how simpler ligands influence the reduction potentials and spectroscopic signatures, enabling the confident correlation of structure, spectroscopy, and behavior [16,17,18,19]. Traditionally, [2Fe-2S] clusters have been synthesized in two ways: cluster assembly or ligand exchange [8,20,21,22]. Cluster assembly entails the reaction between an iron(III) salt, a bidentate thiolate and NaSH. Addition of sulfur to a rubredoxin analogue, $[Fe(SR)_4]^{2-}$, also results in the self-assembly of a [2Fe-2S] cluster [23]. Ligand exchange is another method for accessing new [2Fe-2S] clusters, particularly for clusters that do not have S-based capping ligands. For example, synthetic [2Fe-2S] clusters with capping N ligands were synthesized using the reaction of $[(Fe_2S_2Cl_2)(NEt_4)_2]$ with a deprotonated ligand [16–19]. The resulting clusters have spectroscopic features similar to the biological clusters but have $Fe^{3+}{}_2/Fe^{2+}Fe^{3+}$ couples that are more negative by 0.36 to 1.73 V [16–19,24,25,26,27]. So far, the N-donors in the synthetic compounds have been based on imidazolates and benzimidazolates, and the use of a wider range of donors has been difficult because of the limited number of methods for synthetic access. The development of new synthetic routes, particularly for N-donor ligands that help to understand Rieske and MitoNEET clusters, is of interest. For example, a new route to a [2Fe-2S] cluster is adding elemental sulfur and tetramethylthiourea (tmtu) to an iron amide complex [28].

Diketiminate ligands (for example, $L = MeC[C(Me)N(2,6\text{-}Me_2C_6H_3)]_2$) are well-established supporting groups for low coordinate iron chemistry [29], and we previously reported diiron(II) complexes with a single sulfide bridge [30,31]. However, synthesizing a diketiminate-supported [2Fe-2S] cluster is difficult. In our hands, the ligand exchange method forms L_2Fe as the major product. In this contribution, we describe a method in which elemental sulfur oxidizes a transient iron(I) species to give a diferric [2Fe-2S] cluster. A similar synthesis of a [2Fe-2S] cluster from a diiron(I) species was recently published [32]. The monoanionic diketiminate ligand gives the overall cluster the same charge as Rieske clusters (Figure 1). We characterize both the oxidized ($Fe^{3+}{}_2$) and the rare reduced ($Fe^{3+}Fe^{2+}$) clusters, with an eye toward insight into the biological system.

Materials and Methods

Unless otherwise noted, all manipulations were performed under an inert atmosphere using Schlenk techniques or in an M. Braun N_2-filled glovebox with O_2 levels maintained at or below 1 ppm. All glassware was dried at 150 °C overnight and Celite was dried under vacuum at 200 °C overnight. All solvents, unless otherwise noted, were dried using activated alumina and copper columns and stored over 4 Å molecular sieves. Acetonitrile was stored under 3 Å molecular sieves. THF was dried by distillation from a Na/benzophenone still and stored over 4 Å molecular sieves. C_6D_6 was dried with alumina, vacuum transferred and stored over 4 Å molecular sieves. KC_8 was prepared by heating graphite and elemental potassium at 160 °C for 4 hours under an argon atmosphere. $[LFe(\mu\text{-}Cl)]_2$ was synthesized via a previously published procedure [33]. PPNCl (bis(triphenylphosphine)iminium chloride) and cryptand-2.2.2 were purchased from Sigma Aldrich.

Synthesis of $[LFe(\mu\text{-}S)]_2$ (L = $MeC[C(Me)N(2,6\text{-}Me_2C_6H_6)]_2$)

Under an atmosphere of N_2, $[LFe(\mu\text{-}Cl)]_2$ (360.1 mg, 0.438 mmol) was dissolved in THF (20 mL) to give a yellow solution and then cooled to −100 °C in a liquid nitrogen cold well. Potassium graphite (136.1 mg, 1.007 mmol, 2.299 equiv) was then added as a solid to the stirring solution. The yellow solution turned dark green upon addition. The reaction mixture was stirred for 30 s at −100 °C and then S_8 (27.9 mg, 0.109 mmol, 0.249 equiv) was added. The reaction mixture was warmed to room temperature while stirring and stirred for 2 h at ambient temperature. The volatile materials were removed under reduced pressure to obtain a dark solid. This solid was then dissolved in dichloromethane (30 mL) and stirred for 10 min at ambient temperature. The purple solution was then filtered through Celite, washing with additional dichloromethane (10 mL) until the filtrate ran clear. The solvent was removed under vacuum to provide a black solid. This solid was washed with pentane (10 mL) and dried to give a black solid (291.4 mg, 0.358 mmol, 81.7% yield). The solid was dissolved in a solution of THF and benzene (6 mL, 1:1) then concentrated to 1.5 mL and stored at −40 °C for three days to provide dark green crystals. ^{1}H NMR (500 MHz, C_6D_6, 25 °C): δ 19.5 (6H, α-methyl), 8.7 (8H, *m*-aryl), 4.4 (24H, *o*-aryl), 3.9 (4H, *p*-aryl), −0.4 ppm (12H, β-methyl). UV-vis (CH_2Cl_2, nm, ε in $mM^{-1}cm^{-1}$): 435 (6.1), 556 (6.9). Mössbauer (80 K, mm/s): δ = 0.28, $|\Delta E_Q|$ = 1.14. Anal. Calcd for $C_{44}H_{54}Fe_2N_4S_2$: C, 64.86, H, 6.68, N, 6.88. Found: C, 64.59, H, 6.51, N, 6.78.

Synthesis of $K[LFe(\mu\text{-}S)]_2$

$[LFe(\mu\text{-}S)]_2$ (516 mg, 0.633 mmol) was dissolved in THF (40 mL) to form a purple solution and cooled to −40 °C. Potassium graphite (94.2 mg, 0.697 mmol, 1.10 equiv) was added as a solid to the stirring solution, turning the purple solution a dark brown-green color. The reaction mixture was stirred at ambient temperature for 30 min and then filtered through Celite. The dark red filtrate was concentrated to 25 mL and cooled to −40 °C to yield crystals (409 mg, 0.479 mmol, 76%). ^{1}H NMR: silent. UV-vis (CH_2Cl_2, nm, ε in $mM^{-1}cm^{-1}$): 333 (>15.6), 417 (1.7), 549 (1.2). Mössbauer (80 K, mm/s): δ_1 = 0.46, $|\Delta E_{Q1}|$ = 0.85; δ_2 = 0.73, $|\Delta E_{Q2}|$ = 1.98. Anal. Calcd for $C_{44}H_{54}Fe_2N_4S_2K$: C, 61.89, H, 6.37, N, 6.56. Found: C, 61.86, H, 6.21, N, 6.40.

Synthesis of $[Kcrypt][LFe(\mu\text{-}S)]_2$

$K[LFe(\mu\text{-}S)]_2$ (207 mg, 0.242 mmol) was dissolved in THF (40 mL) and a solution of cryptand-2.2.2 (91.1 mg, 0.242 mmol) in THF (10 mL) was added. The solution was stirred for 1.5 h, and then filtered through Celite. The dark red filtrate was concentrated to 40 mL and cooled to −40 °C to yield crystals (192 mg, 0.156 mmol, 64%). ^{1}H NMR: silent. UV-vis (CH_2Cl_2, nm, ε in $mM^{-1}cm^{-1}$): 343 (>18.8), 448 (2.9), 556 (1.9). Mössbauer (80 K, mm/s) δ_1 = 0.56, $|\Delta E_{Q1}|$ = 1.02; δ_2 = 0.75, $|\Delta E_{Q2}|$ = 1.92. Anal. Calcd for $C_{62}H_{90}N_6Fe_2S_2KO_6$: C, 60.53, H, 7.37, N, 6.89. Found: C, 60.60, H, 7.36, N, 6.79.

Synthesis of $[((C_6H_5)_3P)_2N][LFe(\mu\text{-}S)]_2$

$[LFe(\mu\text{-}S)]_2$ (36.6 mg, 0.0449 mmol) was dissolved in THF (3 mL) to form a purple solution. Potassium graphite (7.9 mg, 0.058 mmol, 1.3 equiv) was added as a solid to the stirring solution, turning the purple solution a dark brown-green color. The reaction mixture

was stirred at ambient temperature for 30 min and then filtered through Celite. The filtrate was a dark red-purple color. To the stirring solution, PPNCl (25.8 mg, 0.045 mmol, 1.0 equiv) was added as a solid. The reaction mixture was stirred at ambient temperature for 30 min then filtered through Celite. The volatile materials were removed under reduced pressure to give a dark red-purple solid (35.0 mg, 0.0259 mmol, 56% yield). ^{1}H NMR: silent. UV-vis (CH_2Cl_2, nm, ε in $mM^{-1}cm^{-1}$): 336 (>12.5), 447 (2.7), 556 (0.52). Mössbauer (80 K, mm/s) $\delta_1 = 0.48$, $|\Delta E_{Q1}| = 1.02$; $\delta_2 = 0.68$, $|\Delta E_{Q2}| = 1.90$. Anal. Calcd for $C_{80}H_{54}Fe_2N_5S_2P_2$: C, 71.00, H, 6.26, N, 5.17. Found: C, 71.72, H, 6.46, N, 4.80.

Spectroscopic techniques

^{1}H NMR data were obtained using a Bruker Avance 400 MHz spectrometer at room temperature. All resonances (δ) are reported in ppm, relative to residual protiated solvent in C_6D_6 (δ 7.16 ppm). Resonances were singlets unless otherwise noted. Infrared data were obtained using a Bruker ALPHA FTIR spectrometer with a platinum ATR attachment inside a N_2-filled glovebox. Samples were in the solid phase, and crystalline samples were ground to ensure uniformity. UV-vis data were collected on an Agilent Technologies Cary 60 UV-Vis spectrophotomer using Schlenk-adapted quartz cuvettes with a 1 mm optical path length. UV-VIS-NIR data were collected on an Agilent Technologies Cary 5000 spectrophotomer using quartz cuvettes with 1 cm optical path length. Elemental analyses were obtained from the CENTC Elemental Analysis Facility at the University of Rochester. Samples were handled in a VAC Atmospheres glovebox under argon and microanalysis samples were weighed with a PerkinElmer Model AD-6 Autobalance and their compositions were determined with a PerkinElmer 2400 Series II Analyzer.

Mössbauer spectra were recorded on a SeeCo Mössbauer spectrometer with alternating constant acceleration. Shifts are relative to iron metal at 298 K. Sample temperature was maintained at 80 K with a Janis Research Company Inc. cryostat. The spectrum was simulated and fit using WMoss (SeeCo) with Lorentzian doublets.

Electron paramagnetic resonance (EPR) data were obtained using a continuous-wave Bruker EleXsys E500 EPR Spectrometer with an SHQ resonator and an Oxford Instruments ESR-900 helium-flow cryostat. Acquisition parameters were as follows: frequency = 9.3865 GHz, power = 0.0020 mW, conversion time = 41 ms, modulation amplitude = 20 G, modulation frequency = 100 kHz, time constant = 41 ms. The signal was simulated using ESIM (E. Bill, Max Planck Institute for Chemical Energy Conversion, Mülheim an der Ruhr, Germany).

Cyclic voltammetry data were recorded using a PINE WaveNow potentiostat inside a N_2-filled glovebox. A Pt ceramic patterned electrode was used as the working and counter electrode. A silver electrode was used as a quasireference. The electrolyte was a 2.0 mM solution of tetrabutylammonium hexafluorophosphate in dry acetonitrile. A scan rate of 100 mV/s was used unless otherwise noted. Potentials were referenced to the Cp_2Fe^+/Cp_2Fe couple using an internal ferrocene standard.

Crystallographic details are given in the Supporting Information. The crystal structures have been deposited in the CCDC with accession numbers 1060312-1060314.

Results and Discussion

$[LFe(\mu\text{-}Cl)]_2$, a previously characterized diiron(II) complex [33], reacts with KC_8 at −108 °C to form an iron(I) solution, and addition of S_8 at this low temperature gives the diferric species $[LFe(\mu\text{-}S)]_2$ (Scheme 1). This is the same reduction method that results in the activation of N_2 if the reduced solution is warmed [34], but the transient iron(I) intermediate can be trapped using elemental sulfur. The oxidation of an iron(I) species with S_8 was very recently reported by Fohlmeister *et al.*, which also gave a neutral $Fe_2(\mu\text{-}S)_2$ cluster [32]. Synthesis of $[LFe(\mu\text{-}S)]_2$ can also be accomplished through the addition of elemental sulfur to [LFe(benzene)], a previously characterized iron(I) complex [35], but this reaction does not go cleanly, making isolation through this method difficult.

The molecular structure of $[LFe(\mu\text{-}S)]_2$ from X-ray crystallography shows a diamond core with tetrahedral iron atoms (Figure 2). The core bond lengths and angles (Table 1) are similar to those reported for other synthetic [2Fe-2S] clusters [24,32,36,37], and biological [2Fe-2S] clusters [8, 38].

Reducing the complex by one electron using KC_8 gives the new mixed valent [2Fe-2S] cluster $K(THF)_4[LFe(\mu\text{-}S)]_2$. We were able to grow single crystals of this compound and of $K(cryptand\text{-}2.2.2)[LFe(\mu\text{-}S)]_2$ (Figure 2). The best stability for spectroscopic studies comes from cation exchange to give $PPN[LFe(\mu\text{-}S)]_2$ (Scheme 2). All mixed valent clusters are ^1H NMR silent. We attribute this to fast relaxation of the protons due to paramagnetism.

The zero field Mössbauer spectrum of $[LFe(\mu\text{-}S)]_2$ fits to one quadrupole doublet with δ = 0.28 mm/s and $|\Delta E_Q|$ = 1.14 mm/s (Figure 3). These values agree with reported values for synthetic diferric [2Fe-2S] clusters [16–19,24–27]. Typical values for nitrogen ligated clusters are δ = 0.24 – 0.28 mm/s and $|\Delta E_Q|$ = 0.87 – 1.26 mm/s. In Rieske clusters, the N-ligated iron has a slightly larger isomer shift of δ = 0.32 mm/s [39,40].

Two quadrupole doublets are observed in the Mössbauer spectrum of $PPN[LFe(\mu\text{-}S)]_2$ (δ = 0.48 mm/s and $|\Delta E_Q|$ = 1.02 mm/s; δ = 0.68 mm/s and $|\Delta E_Q|$ = 1.90 mm/s) (Figure 3), suggesting two different iron environments, and thus the valence is not fully delocalized on the Mössbauer timescale. The isomer shifts in $PPN[LFe(\mu\text{-}S)]_2$ differ by 0.20 mm/s, which suggests partial delocalization of the unpaired electron (Robin-Day Class II) [19,36,41,42]. $K(THF)_4[LFe(\mu\text{-}S)]_2$ (Figure S1) has slightly more localization with a difference in isomer shift of 0.25 mm/s. This may be attributable to the coordination of the cation to the [FeS] core. The difference in isomer shift for $[Kcrypt][LFe(\mu\text{-}S)]_2$ is similar to the PPN analogue, as would be expected with $\Delta\delta$ = 0.19 mm/s (Figure S2). The Mössbauer spectrum of $K(crypt)[LFe(\mu\text{-}S)]_2$ does not change upon increasing the temperature from 80 K to 200 K (Figure S2). The Mössbauer parameters are compared to other synthetic [16–19, 24–27] and biological [37–39] [2Fe-2S] clusters in Table 2.

Alternative fits can be found in the SI for $K[LFe(\mu\text{-}S)]_2$ (Figure S1) and $K(crypt)[LFe(\mu\text{-}S)]_2$ (Figure S2). The alternative fit for $PPN[LFe(\mu\text{-}S)]_2$ has one iron site with δ = 0.34 mm/s and $|\Delta E_Q|$ = 1.22 mm/s, and one with δ = 0.81 mm/s and $|\Delta E_Q|$ = 1.62 mm/s. This fit with $\Delta\delta$ = 0.47 mm/s is further from literature precedents (see above), and inconsistent with the partial delocalization observed by EPR spectroscopy (see below).

At 9.8 K, the X-band EPR spectrum of PPN[LFe(μ-S)]$_2$ (Figure 3) consists of one nearly axial S = ½ signal with **g** = [2.015, 1.921, 1.904] and g_{av} = 1.946. Rieske proteins have g_{av} = 1.90 – 1.91 that are smaller than their symmetrical counterparts, ferredoxins (1.95 – 1.97) [39,43,44], due to the localization of the unpaired electron on one of the iron atoms in the asymmetric cluster. Ferredoxins, which have delocalized valence in the $Fe^{2+}Fe^{3+}$ form, have g_{av} closer to the value of the free electron. The average g-factor of PPN[LFe(μ-S)]$_2$ lies between these values, consistent with partial delocalization like other synthetic mixed valent complexes [16–19,24–27]. As in other isolable synthetic mixed-valence [2Fe-2S] compounds, we observe no intervalence charge-transfer band via UV-Vis-NIR spectroscopy (Figure S7) [16–19,24–27].

The crystal structure of K(crypt)[LFe(μ-S)]$_2$ shows two crystallographically independent molecules. In a key observation, one iron atom has Fe-S bonds that are shorter by ~0.04 Å and Fe-N bonds that are shorter by ~0.02 Å (Table 1), consistent with this site being the more oxidized iron(III) site. Localization of iron sites was previously observed in a $[2Fe\text{-}2S]^+$ cluster with two different supporting ligands [27], where the bonds from sulfide to the N-coordinated iron (Fe_N) were about 0.08 Å longer than those to the S-coordinated iron (Fe_S). This is twice the difference observed in K(crypt)[LFe(μ-S)]$_2$. However, it is more relevant to consider the two previous mixed-valence [2Fe-2S] clusters with identical supporting ligands on each iron center [17,24]. In the first the molecule was found on a crystallographic inversion center, which makes it impossible for the crystal structure to show asymmetry between the iron sites [17]. This phenomenon could mask any asymmetry of the core through static disorder, an idea that was supported in the crystal structure of a very similar compound in which the subsites were crystallographically independent [24], in which the bonds from the bridging sulfides were 0.02–0.03 Å longer to one of the two iron atoms, and the same iron atom also had longer bonds to the supporting ligand.

Interestingly, the two crystal structures of the diketiminate complexes show both situations. The X-ray crystal structure of K(THF)$_4$[LFe(μ-S)]$_2$ has the Fe_2S_2 rhomb lying on a crystallographic inversion center, and necessarily shows equivalent bond distances to the two Fe atoms. However, the crystal structure of the K(crypt) salt has crystallographically independent iron sites, enabling us to distinguish the iron(II) site with the longer bonds from the iron(III) site with the shorter bonds. The crystallographic observation of localization is consistent with the observation of two different doublets in the Mössbauer spectrum. We note in passing that the observation of site localization by X-ray and Mössbauer spectroscopies indicates that the reason for the overall S = 1/2 ground state of the cluster (rather than the S = 9/2 ground state that might be expected with strong double exchange [45,46]) is charge localization, rather than vibronic coupling as previously proposed [47].

Solutions of the new clusters in acetonitrile show a reversible $Fe^{3+}{}_2/Fe^{2+}Fe^{3+}$ couple at −1.00 V vs. Cp_2Fe^+/Cp_2Fe (Figure 4). This redox potential is much closer to biological clusters [48] than other reported synthetic [2Fe-2S] clusters [16–19,24–27] (Table 3). We attribute the relatively positive potential to the fact that [LFe(μ-S)]$_2$ is not anionic like the other synthetic clusters, while the biological clusters have hydrogen bonding to the coordinated thiolates that dissipates negative charge buildup [49]. The only previously published neutral clusters gave irreversible reductions [28,32].

The diferrous state has been observed in a few ferredoxin [52,53] and Rieske [54,55] [2Fe-2S] clusters. This doubly reduced cluster can be stabilized in proteins by protonation or hydrogen bonding to nearby residues [56]. We observe a second quasi-reversible redox event at a more negative potential of −1.36 V. This redox event is tentatively assigned as a $Fe^{2+}Fe^{3+}/Fe^{2+}{}_2$ couple; however, we were unable to isolate the diferrous cluster. Recently, Albers et al. reported the first and only synthetic diferrous [2Fe-2S] cluster [57].

Conclusion

We have discovered a route to [2Fe-2S] clusters from S_8 oxidation of a transient iron(I) species, which opens the door to diketiminate-supported [2Fe-2S] clusters. The single negative charge on the bidentate diketiminate is less than the two negative charges from typical bis(thiolate) or bis(benzimidazole) supporting ligands, and the less negative redox potential makes these clusters easier to handle and study. The spectroscopic characteristics of the mixed-valence $Fe^{3+}Fe^{2+}$ cluster indicate that the electron is only partially delocalized, with spectroscopically and crystallographically distinguishable iron(II) vs. iron(III) sites in the ground state. These results suggest that previous observations of symmetric cores were caused by crystal packing constraints, and that there is site localization in agreement with Mössbauer data.

Supplementary Material

Refer to Web version on PubMed Central for supplementary material.

Acknowledgments

Funding was provided by the National Institutes of Health (GM065313). We thank Eckhard Bill and Wilda Vargas for preliminary experiments, and Richard Lewis for checking reproducibility of the syntheses.

References

1. Beinert H, Holm RH, Münck E. Science. 1997; 277:653–659. [PubMed: 9235882]
2. Beinert H. J Biol Inorg Chem. 2000; 5:2–15. [PubMed: 10766431]
3. Fontecave M. Nat Chem Biol. 2006; 2:171–174. [PubMed: 16547473]
4. Crack JC, Green J, Thomson AJ, Le Brun NE. Curr Opin Chem Biol. 2012; 16:35–44. [PubMed: 22387135]
5. Lill R. Nature. 2009; 460:831–838. [PubMed: 19675643]
6. Kennepohl P, Solomon EI. Inorg Chem. 2003; 42:696–708. [PubMed: 12562183]
7. Sigfridsson E, Olsson MHM, Ryde U. Inorg Chem. 2001; 40:2509–2519. [PubMed: 11350228]
8. Venkateswara Rao P, Holm RH. Chem Rev. 2004; 104:527–560. [PubMed: 14871134]
9. Ferraro DJ, Gakhar L, Ramaswamy S. Biochem Biophys Res Comm. 2005; 338:175–190. [PubMed: 16168954]
10. Wiley SE, Paddock ML, Abresch EC, Gross L, van der Geer P, Nechushtai R, Murphy AN, Jennings PA, Dixon JE. J Biol Chem. 2007; 282:23745–23749. [PubMed: 17584744]
11. Bak DW, Elliott SJ. Curr Opin Chem Biol. 2014; 19:50–58. [PubMed: 24463764]
12. Zuris JA, Halim DA, Conlan AR, Abresch EC, Nechushtai R, Paddock ML, Jennings PA. J Am Chem Soc. 2010; 132:13120–13122. [PubMed: 20812736]
13. Kimura S, Kikuchi A, Senda T, Shiro Y, Fukuda M. Biochem J. 2005; 388:869–878. [PubMed: 15733056]

14. Holden HM, Jacobson BL, Hurley JK, Tollin G, Oh BH, Skjeldal L, Chae YK, Cheng H, Xia B, Markley JL. J Bioenerg Biomembr. 1994; 26:67–88. [PubMed: 8027024]
15. Liu J, Chakraborty S, Hosseinzadeh P, Yu Y, Tian S, Petrik I, Bhagi A, Lu Y. Chem Rev. 2014; 114:4366–4469. [PubMed: 24758379]
16. Ballmann J, Albers A, Demeshko S, Dechert S, Bill E, Bothe E, Ryde U, Meyer F. Angew Chem Int Ed. 2008; 47:9537–9541.
17. Albers A, Demeshko S, Dechert S, Bill E, Bothe E, Meyer F. Angew Chem Int Ed. 2011; 50:9191–9194.
18. Fuchs MGG, Dechert S, Demeshko S, Meyer F. Eur J Inorg Chem. 2010; 2010:3247–3251.
19. Ballmann J, Dechert S, Demeshko S, Meyer F. Eur J Inorg Chem. 2009; 2009:3219–3225.
20. Ballmann J, Sun X, Dechert S, Schneider B, Meyer F. Dalton. 2009:4908–4917.
21. Beardwood P, Gibson JF. J Chem Soc Chem Comm. 1985:1345–1347.
22. Do Y, Simhon ED, Holm RH. Inorg Chem. 1983; 22:3809–3812.
23. Hagen KS, Watson AD, Holm RH. J Am Chem Soc. 1983; 105:3905–3913.
24. Saouma CT, Kaminsky W, Mayer JM. J Am Chem Soc. 2012; 134:7293–7296. [PubMed: 22519585]
25. Albers A, Bayer T, Demeshko S, Dechert S, Meyer F. Chem Eur J. 2013; 19:10101–10106. [PubMed: 23780647]
26. Ding XQ, Bill E, Trautwein AX, Winkler H, Kostikas A, Papaefthymiou V, Simopoulos A, Beardwood P, Gibson JF. J Chem Phys. 1993; 99:6421–6428.
27. Albers A, Demeshko S, Dechert S, Saouma CT, Mayer JM, Meyer F. J Am Chem Soc. 2014; 136:3946–3954. [PubMed: 24506804]
28. Ohki Y, Sunada Y, Tatsumi K. Chem Lett. 2005; 34:172–173.
29. Holland PL. Acc Chem Res. 2008; 41:905–914. [PubMed: 18646779]
30. Vela J, Stoian S, Flaschenriem CJ, Münck E, Holland PL. J Am Chem Soc. 2004; 126:4522–4523. [PubMed: 15070362]
31. Rodriguez MM, Stubbert BD, Scarborough CC, Brennessel WW, Bill E, Holland PL. Angew Chem Int Ed. 2012; 51:8247–8250.
32. Fohlmeister L, Vignesh KR, Winter F, Moubaraki B, Rajaraman G, Pottgen R, Murray KS, Jones C. Dalton Trans. 2015; 44:1700–1708. [PubMed: 25462174]
33. Grubel K, Brennessel WW, Mercado BQ, Holland PL. J Am Chem Soc. 2014; 136:16807–16816. [PubMed: 25412468]
34. Rodriguez MM, Bill E, Brennessel WW, Holland PL. Science. 2011; 334:780–783. [PubMed: 22076372]
35. MacLeod KC, Vinyard DJ, Holland PL. J Am Chem Soc. 2014; 136:10226–10229. [PubMed: 25004280]
36. Hoggins JT, Steinfink H. Inorg Chem. 1976; 15:1682–1685.
37. Iwata S, Saynovits M, Link TA, Michel H. Structure. 1996; 4:567–579. [PubMed: 8736555]
38. Fukuyama K. Photosynth Res. 2004; 81:289–301. [PubMed: 16034533]
39. Fee JA, Findling KL, Yoshida T, Hille R, Tarr GE, Hearshen DO, Dunham WR, Day EP, Kent TA, Münck E. J Biol Chem. 1984; 259:124–133. [PubMed: 6323399]
40. Meyer J, Clay MD, Johnson MK, Stubna A, Münck E, Higgins C, Wittung-Stafshede P. Biochemistry. 2002; 41:3096–3108. [PubMed: 11863449]
41. Day P, Hush NS, Clark RJH. Phill Trans R Soc A. 2008; 366:5–14.
42. Beschoten B, Crowell PA, Malajovich I, Awschalom DD, Matsukura F, Shen A, Ohno H. Phys Rev Lett. 1999; 83:3073–3076.
43. Tiago de Oliveira F, Bominaar EL, Hirst J, Fee JA, Münck E. J Am Chem Soc. 2004; 126:5338–5339. [PubMed: 15113187]
44. Fritz J, Anderson R, Fee J, Palmer G, Sands RH, Tsibris JC, Gunsalus IC, Orme-Johnson WH, Beinert H. Biochim Biophys Acta. 1971; 253:110–133. [PubMed: 4331268]
45. Crouse BR, Meyer J, Johnson MK. J Am Chem Soc. 1995; 117:9612–9613.
46. Achim C, Bominaar EL, Meyer J, Peterson J, Münck E. J Am Chem Soc. 1999; 121:3704–3714.

47. Gamelin DR, Bominaar EL, Kirk ML, Wieghardt K, Solomon EI. J Am Chem Soc. 1996; 118:8085–8097.
48. Colbert CL, Couture MM, Eltis LD, Bolin JT. Structure. 2000; 8:1267–1278. [PubMed: 11188691]
49. Dey A, Jenney FE Jr, Adams MW, Babini E, Takahashi Y, Fukuyama K, Hodgson OK, Hedman B, Solomon EI. Science. 2007; 318:1464–1468. [PubMed: 18048692]
50. Connelly NG, Geiger WE. Chem Rev. 1996; 96:877–910. [PubMed: 11848774]
51. Sawyer, DT., Sobkowiak, A., Roberts, JL, Jr. Electrochemistry for Chemists. Wiley; New York: 1995.
52. Im S-C, Lam K-Y, Lim M-C, Ooi B-L, Sykes AG. J Am Chem Soc. 1995; 117:3635–3636.
53. Yoo SJ, Meyer J, Münck E. J Am Chem Soc. 1999; 121:10450–10451.
54. Verhagen MFJM, Link TA, Hagen WR. FEBS Letters. 1995; 361:75–78. [PubMed: 7890043]
55. Leggate EJ, Bill E, Essigke T, Ullmann GM, Hirst J. Proc Natl Acad Sci USA. 2004; 101:10913–10918. [PubMed: 15263097]
56. Saouma CT, Kaminsky W, Mayer JM. Polyhedron. 2013; 58:60–64. [PubMed: 23976815]
57. Albers A, Demeshko S, Pröpper K, Dechert S, Bill E, Meyer F. J Am Chem Soc. 2013; 135:1704–1707. [PubMed: 23320988]

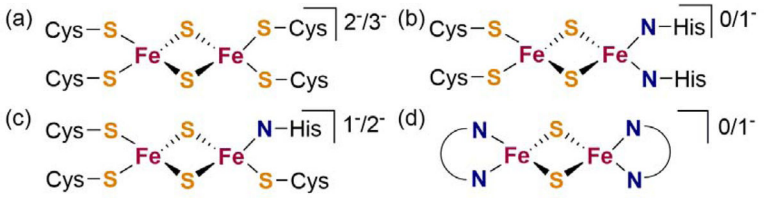

Figure 1.

Core structures of (a) ferredoxin, (b) Rieske type, (c) MitoNEET and (d) $[LFe(\mu\text{-}S)]_2$ [2Fe-2S] clusters.

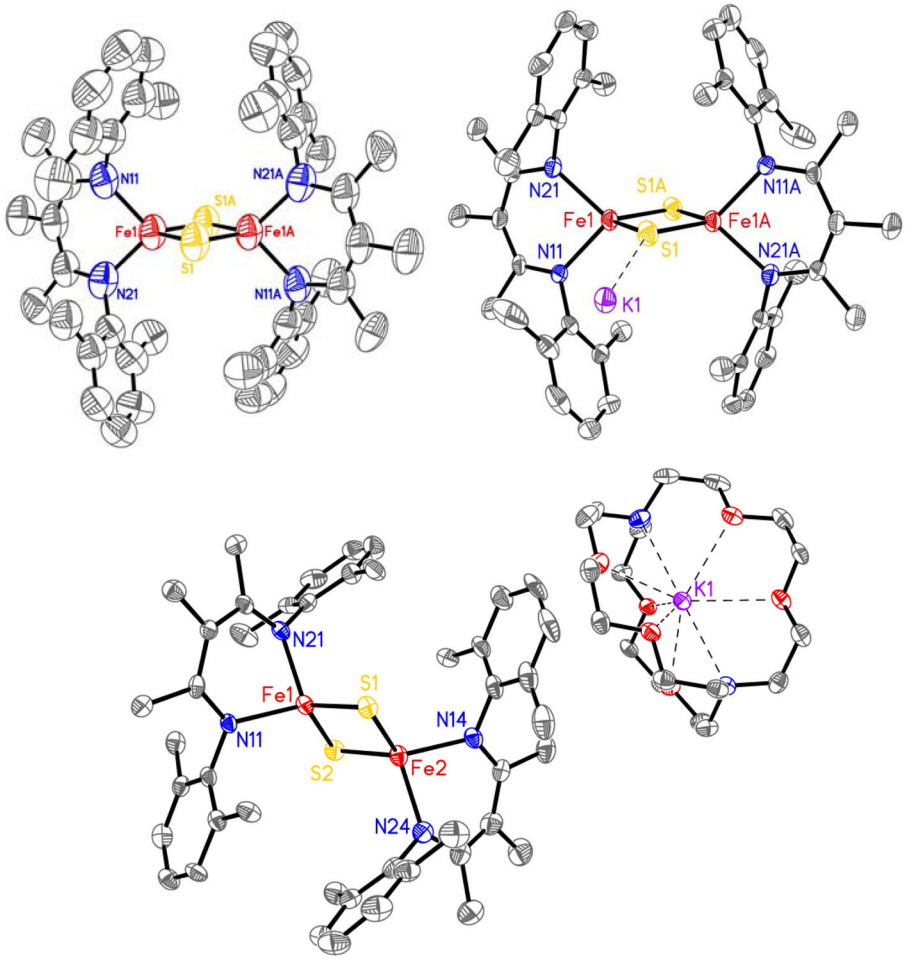

Figure 2.

Plot of $[LFe(\mu\text{-}S)]_2$ (top left), $K(THF)_4[LFe(\mu\text{-}S)]_2$ (top right), and K(cryptand-2.2.2)$[LFe(\mu\text{-}S)]_2$ (bottom) with thermal ellipsoids at 50% probability. Hydrogen atoms, solvent, and second molecule in K(cryptand-2.2.2)$[LFe(\mu\text{-}S)]_2$ unit cell omitted for clarity.

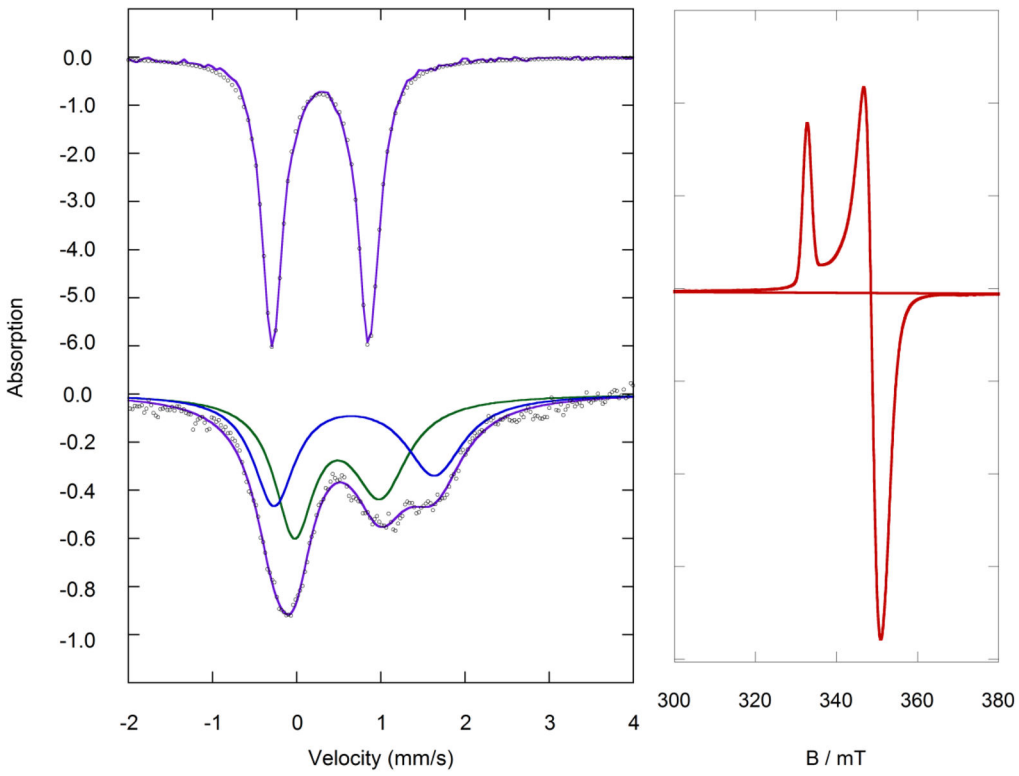

Figure 3.

Left: The zero field Mössbauer spectra of (top) diferric $[LFe(\mu\text{-}S)]_2$ in the solid state at 80 K, and (bottom) mixed-valent $PPN[LFe(\mu\text{-}S)]_2$ as a frozen solution in THF at 80 K. The black circles are the data and the purple lines represent the simulated fits. Right: The derivative X-band EPR spectrum of mixed valent $PPN[LFe(\mu\text{-}S)]_2$ as a 0.2 mM solution in THF at 9.8 K.

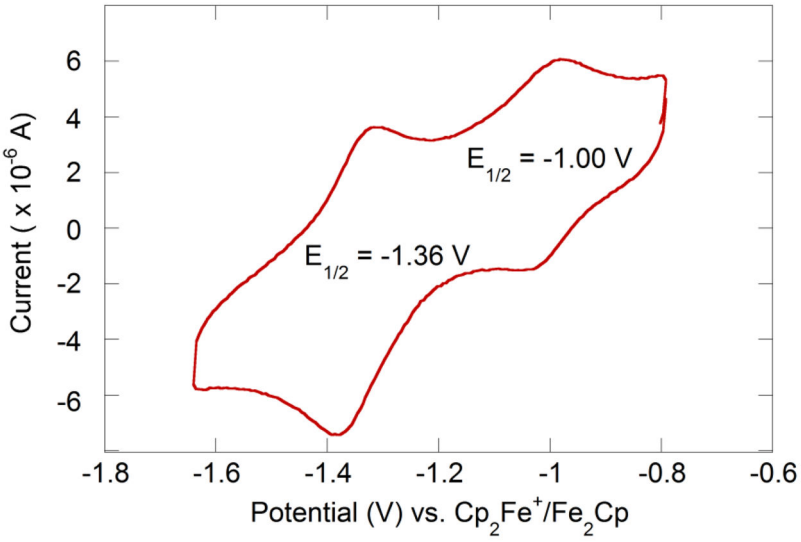

Figure 4.

Cyclic voltammogram of 2.08 mM $[LFe(\mu\text{-}S)]_2$ in acetonitrile with 0.16 M NBu_4PF_6, with a scan rate of 100 mV/s referenced to ferrocene using an internal standard (not shown).

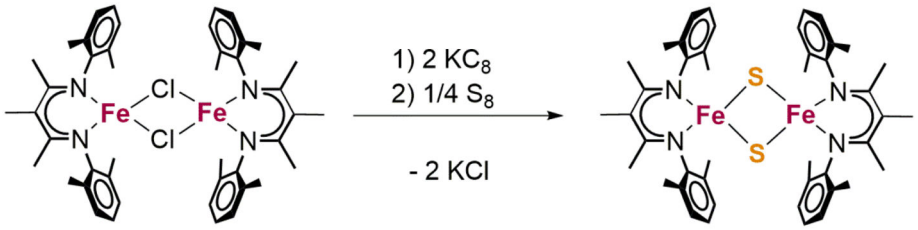

Scheme 1.
Synthesis of $[LFe(\mu\text{-}S)]_2$ from $[LFe(\mu\text{-}Cl)]_2$

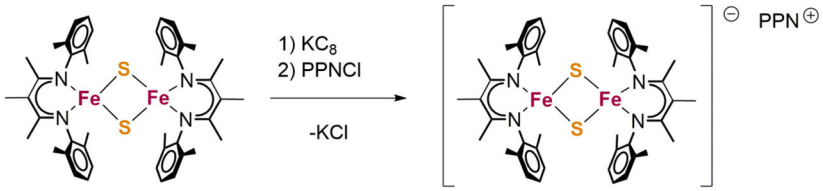

Scheme 2.
Synthesis of PPN[LFe(μ-S)]$_2$

Table 1

Selected bond lengths (Å) and angles (°) for $[LFe(\mu\text{-}S)]_2$, synthetic, and biological [2Fe-2S] clusters

Cluster		d(Fe-Fe)	d(Fe-S)	d(Fe-N)	<(S-Fe-S)	Ref
$[LFe(\mu\text{-}S)]_2$	$2Fe^{3+}$	2.669(1)	2.196(2) 2.212(2)	1.970(5) 1.975(5)	105.49(7)	This work
$K[LFe(\mu\text{-}S)]_2$	$Fe^{2+}Fe^{3+}$	2.723(2)	2.224(2) 2.229(2)	2.016(6) 2.034(4)	104.60(7)	This work
K(crypt) $[LFe(\mu\text{-}S)]_2$	$Fe^{2+}Fe^{3+}$	Fe(1–2): 2.690(1) Fe(3–4): 2.684(1)	Fe(1,3): 2.18–2.22 Fe(2,4): 2.22–2.27	Fe (1,3): 2.016–2.035 Fe(2,4): 2.023–2.043	107.32(6), 104.15(5), 103.79(6), 106.50(6)	This work
$[N\ Fe(\mu\text{-}S)]_2$	$2Fe^{3+}$	2.647(1)	2.18/2.18	2.008/2.012	105.35	32
$[N^1N^2Fe(\mu\text{-}S)]_2$	$2Fe^{3+}$	2.783(2)	2.212(2)/2.421(2)	1.930(5)	101.89(6)	28
$[[N_2Fe(\mu\text{-}S)]_2]^{2-}$	$2Fe^{3+}$	2.7	2.19/2.21	1.89/1.99	104.27	16
	$Fe^{2+}Fe^{3+}$	2.69	2.22/2.23	2.04/2.05	105.8	17
$[[N_2Fe(\mu\text{-}S)]_2]^{2-}$	$2Fe^{3+}$	2.687(1)	2.197	1.978	104.68(6)	24
	$Fe^{2+}Fe^{3+}$	2.7123	2.227	2.048	-	24
$[N_2Fe(\mu\text{-}S)_2FeS_2]^{2-}$	$2Fe^{3+}$	2.694(1)	Fe_N-S: 2.189/2.194 Fe_S-S: 2.200/2.216	1.985(2)/1.988(2)	104.45	27
	$Fe^{2+}Fe^{3+}$	2.682(1)	Fe_N-S: 2.241/2.248 Fe_S-S: 2.210/2.212	2.057(4)/2.212(2)	102.23	27
Rieske, bovine heart *bc*$_1$	$2Fe^{3+}$	2.7	2.24/2.25	2.16/2.13	105.6	37
Ferredoxin, *Anabaena 9119*	$2Fe^{3+}$	2.746	2.278/2.234 2.227/2.184	-	102.2/105.6	

*For entry 4 N_2 = guanidinate ligand; for entry 5 N^1 = $N(SiMe_3)_2$, N^2 = tetramethylthiourea; entries 6 and 7 N_2 = bis(benzimidazolate) ligand; entry 8 N_2 = bis(benzimidazolate) and S_2 = 1,1′-biphenyl 2,2′-dithiolate.

Table 2

Mössbauer data for [2Fe-2S] clusters.

Cluster	Oxidation States	δ (mm/s)	$\|\Delta E_Q\|$ (mm/s)	T (K)	Ref
$[LFe(\mu\text{-}S)]_2$	$2Fe^{3+}$	0.28	1.14	80	This work
$PPN[LFe(\mu\text{-}S)]_2$	$Fe^{2+}Fe^{3+}$	0.48	1.02	80	This work
		0.68	1.90		
$K(THF)_4[LFe(\mu\text{-}S)]_2$	$Fe^{2+}Fe^{3+}$	0.46	0.85	80	This work
		0.73	1.98		
$[N_2Fe(\mu\text{-}S)]_2]$	$2Fe^{3+}$	0.15	1.92	78	32
$[[N_2Fe(\mu\text{-}S)]_2]^{2-/3-}$	$2Fe^{3+}$	0.24	0.87	80	17
	$Fe^{2+}Fe^{3+}$	0.47	1.41	80	
		0.69	2.90		
$[[N_2Fe(\mu\text{-}S)]_2]^{2-/3-}$	$2Fe^{3+}$	0.27	0.90	80	26
	$Fe^{2+}Fe^{3+}$	0.43	1.53	80	
		0.68	2.86		
Thermus thermophilus Rieske cluster	$2Fe^{3+}$	0.24	0.52	4.2	39
		0.32	0.91		
	$Fe^{2+}Fe^{3+}$	0.22	0.61	230	
		0.65	2.81		
Aquifex geolicus ferredoxin cluster	$2Fe^{3+}$	0.26	0.62	4.2	40
		0.28	0.76		
	$2Fe^{3+}$	0.30	1.00	4.2	
		0.62	3.00		

*For entry 4, N_2 = guanidinate ligand; entries 5 and 6, N_2 = bis(benzimidazolate)

Table 3

Redox potentials for [2Fe-2S] clusters

Oxidized Cluster	**$Fe^{3+}{}_2/Fe^{3+}Fe^{2+}$ (V)[a]**	**$Fe^{3+}Fe^{2+}/Fe^{2+}{}_2$ (V)[a]**	**Ref**
$[LFe(\mu\text{-}S)]_2$	−1.00	−1.36	This work
$[N_2Fe(\mu\text{-}S)]_2{}^{-2}$	−1.23	−2.20	17
$[N_2Fe(\mu\text{-}S)]_2{}^{-2}$	−1.43	−2.19	27
$[N_2Fe(\mu\text{-}S)_2FeS_2]^{-2}$	−2.38	-	16
$[N_2Fe(\mu\text{-}S)_2FeS_2]^{-2}$	−1.21	−2.17	25
Protein type	$Fe^{3+}{}_2/Fe^{3+}Fe^{2+}$ (V)[b]		Ref
Ferredoxin	−0.85 to −0.65		48
Rieske	−0.56 to −0.04		49

[*] For entries 2–5, N_2 = bis(benzimidazolate) ligand; for entries 4 and 5, S_2 = 1,1′-biphenyl 2,2-dithiolate ligand

[a] All reduction potentials referenced to $[FeCp_2]^{0/+}$. Entry 4 is referenced to $[FeCp_2{}^*]^{0/+}$ and converted with E° = −0.48 V vs $[FeCp_2]^{0/+}$ in acetonitrile [50].

[b] Protein values referenced to $[FeCp_2]^{0/+}$ using E° = +0.40 V. vs. SHE in water [51]. SHE = standard hydrogen electrode.